journal

J. Am. Ceram. Soc., 87 [8] 1446–1453 (2004)

High-Frequency Electromagnetic Bandgap Structures via Indirect Solid Freeform Fabrication

Christopher J. Reilly,*,†,§ William J. Chappell,‡ John W. Halloran,**,† and Linda P. B. Katehi‡

Advanced Ceramics Laboratory, Department of Materials Science and Engineering, University of Michigan, Ann Arbor, Michigan 48108

Radiation Laboratory, Department of Electrical Engineering and Computer Science, University of Michigan, Ann Arbor, Michigan 48108

The indirect solid freeform fabrication process is used to fabricate low-loss complex geometry periodic dielectrics for use in the microwave range. Relevant processing details, such as mold fabrication, slurry rheology, curing, and binder burnout, are discussed. Woodpile electromagnetic bandgap structures exhibiting a −40 dB well were shown to be operational at frequencies >110 GHz. Novel designs of planar periodic dielectric resonators with $Q = 965$ at 33 GHz (Q = ratio of the power stored to power lost in the resonator) were realized in alumina. Metallo-dielectric filters with low-insertion loss were also created via ISFF; modeling of these structures using resistor-inductor-capacitor-equivalent circuit analysis was performed to calculate a Q of 645.

I. Introduction

First proposed by Yablonovitch,[1] it is now well-known that periodic dielectric structures can act to block the propagation of an electromagnetic wave. The periodicity acts as a bandstop, multidimensional spatial filter because energy will evanesce into the material over a range of frequencies instead of propagate. Both two- and three-dimensional structures have been proposed that exhibit this effect.

By removing one of the periodic inclusions in an electromagnetic bandgap (EBG) structure, a defect periodic structure[2] and accompanying defect mode resonance can be created. The resonance can be used by coupling multiple defects, creating a high-quality filter useful for microwave front-end modules.

Early attempts at realizing three-dimensional EBG structures were face-centered cubic arrays of dielectric spheres in foam.[3] As an advance over this earlier EBG structure, Ozbay[4] first proposed stacked arrays of rods, commonly referred to as woodpiles. The woodpile is known to have a bandgap in which propagation is prohibited and all incident energy is reflected for all angles of incidence for all polarizations.[5] Low-frequency woodpiles were of interest because of their ease of prototyping using manually stacked dielectric rods.[5] Also, micro-machined silicon wafers were stacked to create a higher frequency 3-D woodpile in 1994.[6] Researchers at Sandia National Labs[7] successfully manufactured lithographically defined woodpiles of polycrystalline silicon that were functional at high frequency (90 to 500 GHz) but limited in applicability because of the high-loss tangent of the silicon dielectric.

In addition, a two-dimensional EBG substrate can be created using a square array of alumina rods embedded in air, supported by two thin ceramic layers to both maintain the relative location of the rods and provide a substrate surface for subsequent processing steps. In the present application, the thin layers are metallized to create a parallel plate. An EBG defect resonator is made by intentionally interrupting the otherwise periodic lattice.[8] The defect localizes energy within the lattice and a resonance is created. As an alternative to the periodic dielectric rods, a metallo-dielectric bandgap has been proposed in which periodic metal rods will contain energy in two-dimensions, displaying a low-stop effect. Energy is blocked from dc to an upper cutoff because of the two-dimensional array of metallic inclusion in a parallel plate. The relevant electrical aspects of these structures are the focus of a recent paper,[9] and the focus of this paper is to elucidate manufacturing methodologies for the successful realization of the proposed structures.

In each type of periodic structure, a critical component is the loss of the material. In many applications, the beneficial aspect of the periodic structure is the ability to localize or reflect energy using a dielectric instead of metal. The effect is beneficial only if the material is low loss at the microwave frequencies of interest. The use of a lower dielectric loss material in the periodic structure will result in a sharper resonance of the defect mode. The use of a low-loss material in a filter structure lessens the trade off between insertion loss and bandwidth. Therefore, improving microwave filters is in many ways a materials issue. The development of the periodic structures out of a low-loss material is imperative for beneficial integration into high-frequency systems.

However, there are relatively few methods to manipulate low-loss, high-frequency materials. To this end, we apply the indirect solid freeform fabrication (ISFF) method to high-purity alumina EBG woodpile structures, planar EBG substrates, and metallo-dielectric filters. The low-loss properties of the alumina allow for a higher quality resonance in the defect mode of the substrates. The ISFF process involves the suspension polymerization casting of a ceramic-loaded suspension into a lost mold fabricated by a rapid prototyping tool. This work builds on previous progress made toward the development of direct fabrication of ceramic parts via both inkjet deposition techniques[10–13] and FDM.[14,15]

Suspension polymerization casting (SPC) is known as an effective way to build complex ceramic parts. In SPC, ceramic powder is mixed with monomers, dispersants, and solvents. The monomer solution is polymerized *in situ*. The ceramic particles are entrapped in the polymer gel network and a ceramic green body is formed as a result of polymerization. Ceramic bodies are created via the subsequent removal of the organic binder system and sintering of the powder compact. Patented by Venkataswamy *et al.*,[16] SPC has been successfully applied to many ceramic systems.[17,18]

R. H. French—contributing editor

Manuscript No. 10072. Received April 9, 2003; approved April 8, 2004.
Supported by NSF Contract No. DMR-9972620.
*Member, American Ceramic Society.
**Fellow, American Ceramic Society.
†Advanced Ceramics Laboratory.
‡Radiation Laboratory.
§Current contact information: creilly@adaptivematerials.com.

A brief overview of the ISFF process follows. The part to be built is first created as a solid body in AutoCAD, and then a modified Boolean negative of the part is translated to .stl format so it can be built on a 3-D inkjet printer (Model MM6Pro, Solidscape, Merrimack, NH) and used as a lost mold in the casting process. The slurry that is cast and cured into the lost mold is 54 vol% alumina, and is formulated using acrylate monomers chosen for their chemical compatibility with the mold material and low toxicity. Once the slurry is cured in the mold to form the green part, it is put through one slow heating cycle to thermally remove the mold and binder and a second cycle to sinter the ceramic.

II. Experimental Procedures

(1) Mold Design and Fabrication

The planar all-dielectric resonator structure consists of two parallel alumina plates separated by an array of alumina rods. For ideal part performance, the plates should be kept as thin as possible. The smallest thickness of the plates formed in the casting process is limited by the ***z***-axis resolution of the build tool used to make the mold. For the 3-D inkjet printer, the layers are 50.8 μm thick. To ensure continuity of the plates and the stability of the structure, the molds are made such that the plates are 250 μm thick after casting.

The feature size resolution of the final part is limited by the mold-making tool and the size scale of the part determines its frequency range of operation. As the wavelengths of the radiation for the microwave bands of interest in air are on the order of a few millimeters, the molds for these structures are well within our range of manufacturing capability.

(2) Slurry Formulation and Rheology

The monomer solution used in the formulation of the alumina slurry is a 7:1 mix of isobornyl acrylate (IBA; Sartomer 506, Aldrich, Milwaukee, WI) to propoxylated neopentyl glycol diacrylate (PNGPDA; Sartomer 9003, Aldrich) which is diluted by 20 vol% with decahydronapthalene (Decalin, Avocado Research Chemicals Ltd., Heysham, U.K.). The alumina is A-16SG (Alcoa, Pittsburgh, PA) powder with median particle size (D_{50}) of 0.4 μm. The density of the powder is 3.92 g/, and the specific surface area of this powder is 9 m^2/g. 3 wt% CC-55 (Witco, Houston, TX) surfactant is used as a dispersant for this system.

A stable, low-viscosity slurry with high-solids loading is essential to successful ISSF. The slurry must be fluid to ensure mold replication, and it must be of high enough solids loading so the part can be sintered to full density after the binder is removed. The incentive for applying suspension polymerization casting techniques toward the fabrication of periodic dielectric structures is that it provides a means of manipulating low-loss ceramics. Several high-volume-solids loadings alumina IBA/PNGPDA/Decalin slurries were prepared and tested. One initial batch of 60 vol% alumina IBA/PNGPDA/Decalin suspension was formulated and diluted back down to 58, 56, 52, 50, and 40 vol% by mixing in additional monomer solution. The rheological properties of the suspensions were measured by a rheometer with concentric cylinder C14 (Bohlin CS-50, Cranbury, NJ). The slurry was agitated for 10 s at room temperature before starting the measurement. The viscosity was measured and recorded as the shear rate was increased.

(3) Curing, Binder Removal, and Sintering

The curing kinetics of alumina slurries formulated with acrylate monomers has been studied, with the autocatalytic polymerization and effect of the alumina filler previously reported.[19] The presence of the decalin has been shown to decrease the double-bond concentration while increasing the reactivities of the monomers and the chain mobility.[20] Benzoyl peroxide (BPO, Aldrich) was selected as an initiator and a catalyst, n,n,dimethyl-p-toluidine, (NNDPT, Aldrich) is used to raise the reaction rates at lower temperatures to preserve the low-melting temperature mold.

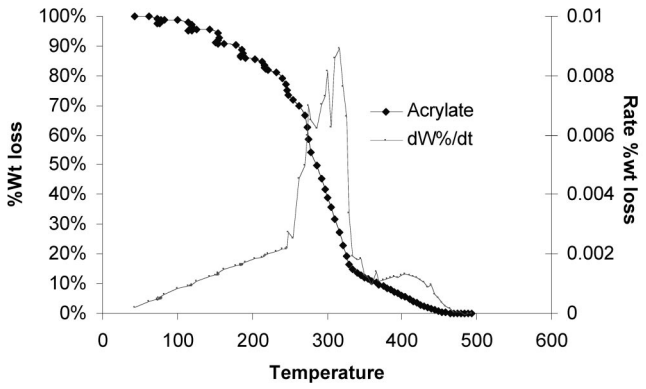

Fig. 1. Thermogravimetric analysis of polymerized acrylates showing weight loss and as a function of temperature.

The pyrolysis behavior of the polymerized sample was characterized by the thermogravimetric analysis (TGA; Model TG171, Cahn, Madison, WI). An air atmosphere was used and the heating rate was set as 10°C/min. The data were collected during the heating process. After reaching 600°C, the instrument was cooled down. The data are plotted in Fig. 1. This plot shows that the acrylate binder system can be completely removed through a simple heating regimen. The TGA records the weight loss of the sample as the temperature increases. It makes apparent the temperature regions of steepest weight loss. The weight of the sample drops as the pyrolyzed binder system leaves the sample. A higher rate of weight loss implies a higher mass-flow rate of organic species. If more species are volatized than can leave the system, cracks are likely to form. To lessen the potential of crack formation, the temperature ramp is slowest when the mass loss is most rapid. To this end, a multiperiod heating ramp to 700°C is used to thermal remove the binder.

Binder-free parts were placed between two flat alumina plates with coarse alumina setter bed powder above and below the part and heated 5°C /min to 1600°C for 4 h. The setter bed acts as a moveable boundary to allow for part shrinkage while maintaining the part between two flat plates during sintering.

Electrical testing of the EBG structures fabricated by ISFF is done with a sweeping signal source network analyzer (Model HP 8522D, Hewlett-Packard, Palo Alto, CA) for structures operating in the frequency range 0–40 GHz, and an anotehr analyzer (Model HP 8510, Hewlett-Packard) is used to obtain frequency sweeps from 40–60 and 75–110 Ghz.

III. Results and Discussion

The viscosity versus shear rate plots for the 58, 56, 52, 50, and 40 vol% alumina slurries are shown in Fig. 2. All tested slurries

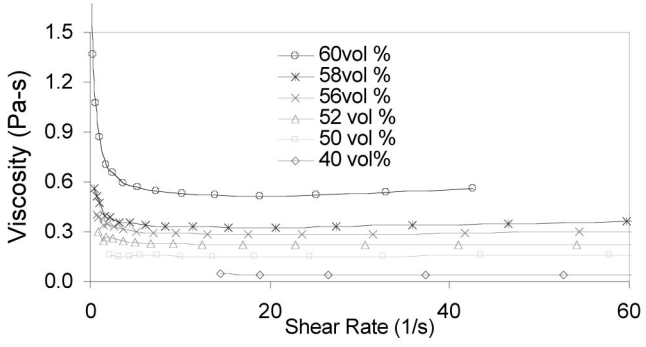

Fig. 2. Viscosity versus shear rate for the alumina slurries of different solids loadings.

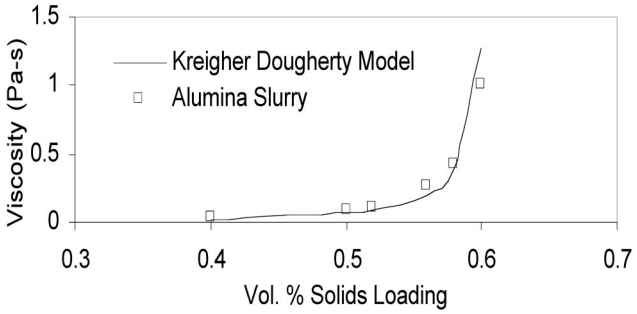

Fig. 3. Viscosity at 10 s^{-1} shear rate versus solids loading for alumina slurry along with Kreiger-Dougherty model fit with B = 1.035.

exhibit a shear thinning behavior at low shear rates and are Newtonian at higher shear rates, >10 s^{-1}. The particles in the unagitated suspension are lightly agglomerated and a small amount of shear stress is required to break up the particle flocculation. This is observed as a high viscosity at low shear rates. Breaking up the agglomerations frees trapped monomer solution and further fluidizes the suspension. As the shear increases, more flocculations are broken up, and the viscosity is observed to drop. When the shear becomes insufficient to further liberate trapped monomer solution via deagglomeration, the viscosity will not change even as the shear rate continues to increase. This behavior is observed at shear rates >10 s^{-1}. The particles are not interacting, but they are a restriction to free fluid flow; therefore, the viscosity of the loaded suspension is higher than an unloaded monomer solution. As the 60, 58, and 56 vol% slurries reach shear rates approaching 50 s^{-1}, the viscosity is observed to increase slightly with increasing shear rate. This shear-thickening behavior is indicative of particle interactions caused by the high shear state of the fluid medium. As the organic liquid is forced into higher shear rates, more particle collisions and interactions are induced, which gives rise to the observed increase in viscosity.

Characterization of the slurry rheology at various solids loadings and shear rates also provides insight into the suspension structure and efficacy of the dispersant system. The dependence of slurry viscosity on the solids loading and initial viscosity of the medium as modeled by Kreiger-Dougherty is given by:[21]

$$\eta = \eta_0\left(1 - \frac{\beta\phi}{\phi_0}\right)^{-2.5\phi_0} \quad (1)$$

Where η is the viscosity of the suspension, η_o is the viscosity of the unloaded liquid, ϕ is the volume fraction of the powder dispersed in the suspension and ϕ_0 is the theoretical maximum packing fraction, typically 0.64 for random close packing of monomodal particles. β is the effective packing factor of the powder in the suspension; it represents a deviation from the idealized hard sphere model ($\beta = 1$) wherein flocculated particles have trapped liquid medium, resulting in an increased effective phase volume of ceramic particles and attendant viscosity.[22] The exponent 2.5 is appropriate for spherical particles.

Figure 3 shows the viscosities measured at high shear rate for the 60, 58, 56, 52, 50, and 40 vol% alumina slurries as a function of the solids loading along with a Kreiger-Dougherty (Eq. (1)) model fit to the data with an effective packing factor value B = 1.035. As previously discussed, B provides insight into the effectiveness of the dispersant and the ideality of the slurry. The B value can be used to estimate the adsorbed layer of dispersant plus trapped monomer solution (*b* in Eq. (2)) surrounding the ceramic particle of diameter *d*.[23]

$$B = \left(1 + \frac{2b}{d}\right)^3 \quad (2)$$

Using Eq. (2) and the B = 1.035 from the empirical fit of the Kreiger Dougherty (Eq. (1)) model to the viscometry data for the alumina slurry gives an adsorbed surfactant layer thickness of *b* = 2.3 nm. This is the same order of magnitude though slightly lower than values obtained by other researchers.[23,24] This implies that there is less monomer solution trapped near the particles in this alumina slurry, giving a lower effective phase volume of solids and slurry behavior that is closer to "hard-sphere" ideality. Viscosity measurements and analysis suggest that the surfactant used in this process is a very effective dispersant for this system. Based on these measurements, a 54 vol% solids loading slurry was chosen as the ideal choice to balance the dual requirements of slurry fluidity and green body sinterability.

The results of the ISFF process as applied to periodic dielectric structures are the topic of this section. Figure 4 shows an image of the CAD file of the 35 GHz woodpile structure (a) and the same part realized in alumina (b). An SEM micrograph is shown in Fig. 4(c) to illustrate the rod spacing. For the 35GHz woodpile, the rod size is 1 mm with an intralayer period of 3.74 mm. There are 14 rods in each layer. The individual layers are stacked vertically with a stacking sequence of *a-b-c-d* in which layers *b* and *d* are spun 90° relative to layers *a* and *c*. Layers *a* and *c* (the two layers in the four-layer sequence that are aligned) are offset by roughly half of the intralayer period. The same is true for layers *b* and *d*. The four-layer stack is repeated three times to yield a structure that is 12-rod layers high. Changing the rod size to 0.40 mm and the intralayer period to 1.5 mm shifts the operational frequency range to 90 GHz.

An image of the CAD file of the 2-D defect resonator is shown in Fig. 5(a). The final alumina part fabricated via ISFF is shown in Fig. 5(b). This structure is created using alumina rods embedded in air, supported by two thin ceramic layers to maintain the relative location of the rods. The structure is comprised of a 2-D array of 1.16-mm rods spaced on a square lattice of 3.28 mm. The structure

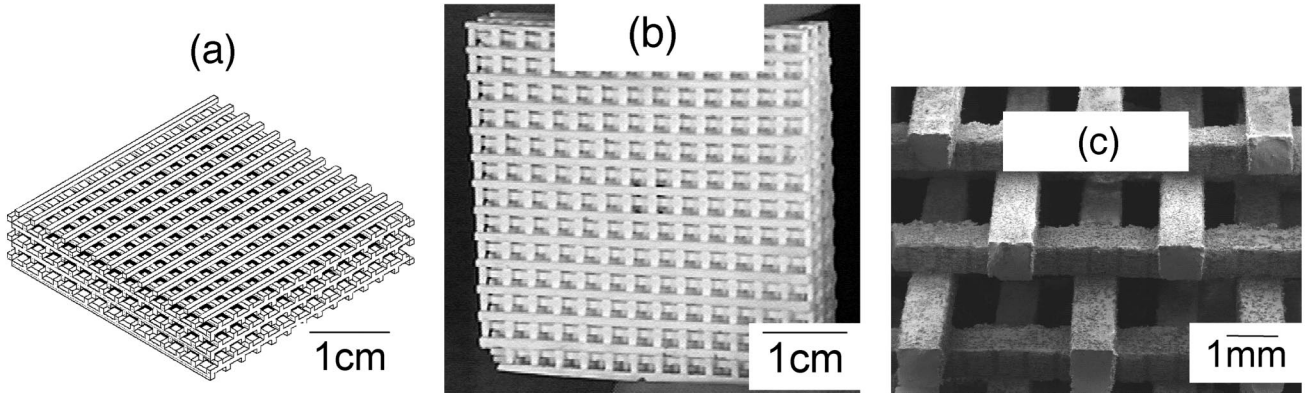

Fig. 4. 35-GHz woodpile electromagnetic bandgap structure: (a) CAD file, (b) optical image of alumina part built via ISFF, and (c) SEM to illustrate rod spacing.

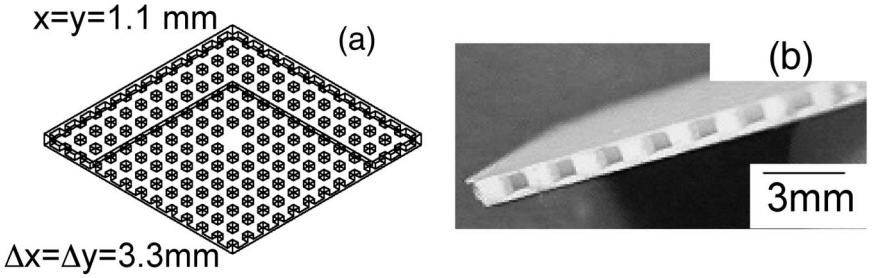

Fig. 5. 2-D planar, all-dielectric defect resonator (a) CAD file, and (b) part realized in alumina via ISFF.

is defected to create a resonance by removing the centermost rod. The parallel plates of dielectric that hold the rods together are ~250 μm thick, but they are polished down to be as thin as possible before device testing.

Figure 6 shows the CAD file of the two-pole metallo-dielectric structure. It consists of 0.9-mm radius metal rods arranged in a rectangular array through a host of dielectric alumina. The array spacings are 4.0 mm in *y* and 3.1 mm in *x*. Metallo-dielectric resonators have one defect, whereas filters have two coupled defects. The resonator structure is defected by removing one metal rod (replaced with dielectric). Multiple periodic inclusions, two in this case, are removed to form a filter from these resonators. The two resonant regions, i.e., the removed elements, are separated in *x* by one unchanged metal rod.

(1) ISFF Alumina Quality

The density of sintered alumina processed via ISFF was measured to be 98.2% of the manufacturer reported value of 3.92 g/cm^3 using the standard Archimedes technique. The microstructure of a sintered specimen that had been polished and thermally etched is pictured in Fig. 7. The alumina ceramic fabricated by ISFF had a final sintered grain size of 3.3 μm. The most important metric for gauging the quality of the alumina fabricated by ISFF for use in periodic dielectrics is the loss characteristics of the material.

Impurities in the alumina would be a potential source of dielectric loss in the final part. To this end, X-ray analysis of fired ISFF alumina was performed before and after processing to determine the effect of the processing scheme on the phase purity of the ceramic. Fully sintered, all-dielectric resonators were reground into powder using a mortar and pestle. The resulting powder was scanned in an X-ray diffractometer (Rotaflex, Rigaku, Tokyo, Japan). The X-ray results from the reground and as-received powder are shown in Fig. 8. The peaks are labeled in agreement with the Joint Committee on Powder Diffraction Standards for alumina. (Powder Diffraction File Card No. 71-1125, International Centre for Diffraction Data, Newtown Square, PA). Expected impurities for the alumina (Na_2O, Fe_2O_3, SiO_2, and B_2O_3, and MgO) do not manifest themselves in phase amounts detectable by X-ray analysis, as they are low-concentration contaminants.

In many fabrication processes, there exists the potential for the quality of the material to degrade. Therefore, a partially filled cylindrical cavity method was used to test the loss properties of the alumina fabricated via ISFF. The resonant frequency of an empty cylindrical cavity was measured and compared with a cavity with a small piece of ISFF alumina placed inside the cavity. The shift in the resonant frequency can be related to the real part of the dielectric constant of the material. The change in resonance of the cavity can be used to evaluate the loss in the material. The results are shown in Fig. 9. A finite-element method (FEM) simulation tool (High Frequency Simulation Software (HFSS) V.7.0, Ansoft, Pittsburgh, PA) was used to determine the relationship between these parameters. This partially filled cavity analysis has calculated the loss tangent of the ISFF processed alumina to be at most 1.7 e-4, which leads to a dielectric, $Q_{\text{dielectric}}$, of ~6000, where Q is a ratio of the power stored to power lost in the resonator, roughly equal to the inverse of the loss tangent of the dielectric when the dielectric loss is the main source of loss in the structure. This $Q = 6000$ is a vast improvement over what can be commercially purchased for milling and shaping into periodic substrates. For example silicon, which can be micromachined, has a maximum $Q_{\text{dielectric}}$ of 1000, which then further degrades when it is processed. Rogers Duroid 6002 (glass filled fluoropolymer) has been used in the past because of its machinability but it limited by a $Q_{\text{dielectric}}$ of only 330.

The loss tangent of alumina is quoted as 1×10^{-4}, giving a homogeneous substrate a $Q_{\text{Dielectric}}$ of 10 000. The loss of the alumina fabricated by ISFF was determined to be 1.7×10^{-4} which yields a $Q_{\text{Dielectric}}$ of ~6000. The less-than-optimal loss properties of the alumina may be in part caused by impurities not detected in the X-ray analysis, or by charges present on the surfaces of the 1.8% residual porosity present in the ceramic.

(A) Fabrication Fidelity: Before testing the electrical performance of the dielectric parts the accuracy of the part fidelity relative to the design was gauged by comparing orthogonal views of the CAD file to orthogonal views of the 35 Ghz woodpile specimen. The density slice function within NIH image photographic analysis software was used to capture the appropriate view

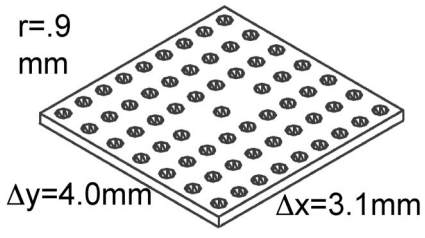

Fig. 6. CAD file of two-pole metallo-dielectric filter structure.

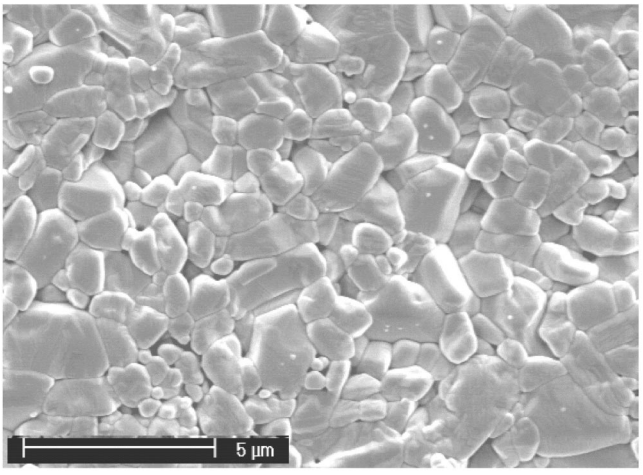

Fig. 7. The microstructure of a thermally etched, sintered specimen of ISFF alumina.

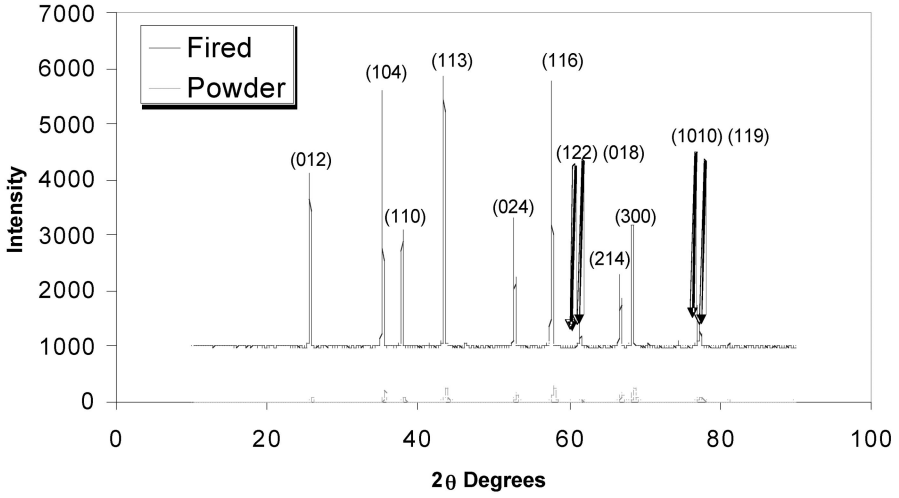

Fig. 8. X-ray diffraction results from the as-received powder and fired ISFF alumina. Peaks are labeled in accordance with Powder Diffraction Card No. 71-1125.

of the CAD file and the corresponding part view from an optical image of the woodpile. The NIH image software was used to calculate the areas of the individual regions and the magnitude of the vectors between feature area centers for both the CAD and alumina part.

The average of the absolute value of the deviation between corresponding vectors for a given view provides an overall figure of merit for the variation in feature placement between the CAD design and the alumina part for that view. The mismatch in magnitudes of corresponding feature areas are also calculated to quantify the structural discrepancy between the design and the fabricated part.

Figure 10 shows the results for this fidelity analysis when applied to the three orthogonal views of the 35 GHz woodpile structure. The average of the variation in the 3.74-mm structural feature placement vector for the three views is 0.93%, with a range of 3.67–3.79 mm. The major cause of discrepancy between CAD image and fabricated part is because of a small amount of curvature present in the woodpile structure because it is being insufficiently supported during sintering. The average of the mismatch in structural feature area (1 mm^2) for the side view is 1.70% with a range of 0.982–1.023 mm^2. Comparison of feature areas for the other views was not performed. To aid in the visualization of the CAD/alumina comparison, the features of the CAD layer have been overlaid on top of the corresponding views of the alumina woodpile. The deviations of the fabricated 3-D alumina woodpile part from the CAD file is comparable to tolerances obtained via common powder processing techniques (±2%).[25]

(2) Electrical Performance of EBG Structures

(A) Three-Dimensional Woodpile Structures: A sweeping signal source network analyzer (Model HP 8522D, Hewlett-Packard) was used for structures operating in the frequency range 0−40 GHz, and the Model HP 8510 (Hewlett-Packard) was used to obtain frequency sweeps from 40−60 and 75–110 Ghz. The woodpile EMB structure under test is mounted between horn antennas as the network analyzer sends and receives signal. This equipment is used to record the power density of the EM wave at each port.

Figure 11(b) shows the transmission versus frequency plot for the 35 GHz woodpile, in which the rod size is 1 mm with an intralayer period of 3.74 mm. The ***x***-axis is a subset of the frequency sweep sent out by the HP 8522D. The ***y***-axis is the ratio of the power received to the power sent, in decibels. The decibel (dB) scale is logarithmic because the ratio of the two can be quite large. Two transmission versus frequency sweep experiments are performed, one with the woodpile between the two horn antennas and one without. The ratio of the power received to the power sent is recorded and plotted in each case. In the case where there is no woodpile EM bandgap structure between the horns, the signal experiences no attenuation. The ratio of power received to power sent is 1, or 0 dB. In the case where the signal is forced to go through the woodpile EM bandgap structure, the attenuation is significant. The ratio of power received to power sent is −40 dB, or <1/10 000 of the signal that is sent from port 1 is received at

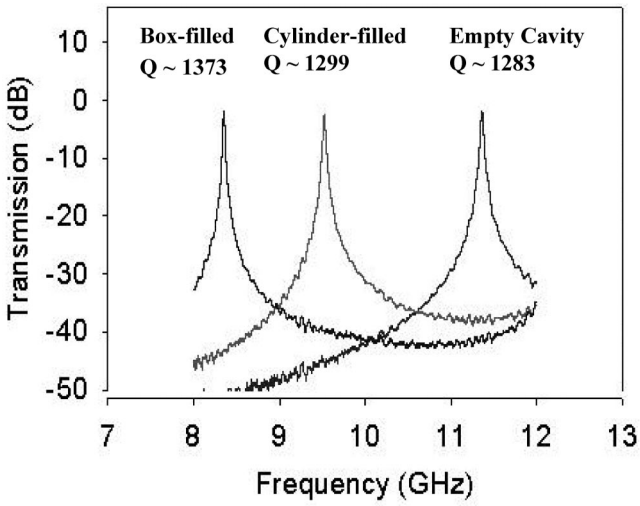

Fig. 9. Transmission versus frequency data for the partially filled cavity analysis to calculate the loss tangent of the ISFF alumina.

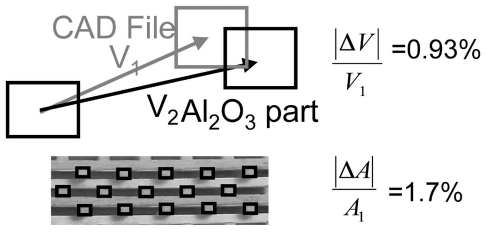

Fig. 10. The mismatch in feature placement vector and feature area between the CAD file and fabricated alumina part is used to gauge the fidelity of the ISFF process.

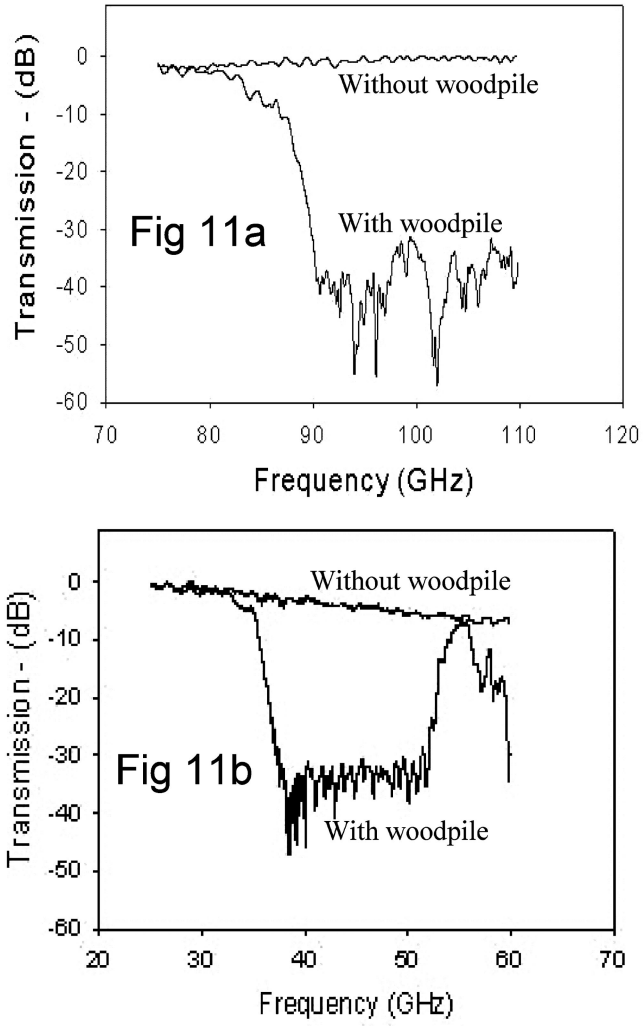

Fig. 11. Measured transmission versus frequency data for the (a) 90-GHz woodpile electromagnetic bandgap structure and (b) 35-GHz woodpile electromagnetic bandgap structure.

port 2. This −40 dB-deep stopband is shown to initiate blocking energy at a frequency of 35 GHz. The bandgap is present up until the end of the measurement range of the equipment, 40 GHz. The HP8510 sweeping signal source network analyzer is substituted for the HP8522D so the transmission versus frequency sweep can be continued up to a high enough frequency to observe the end of the bandgap. At a frequency of ~55 GHz, the transmission of electromagnetic energy is again allowed to propagate from source to receiving antenna.

The HP8510 was also used to provide the EM energy for a transmission versus frequency sweep experiment with the 90 GHz woodpile between the antenna horns. Figure 11(a) shows the transmission versus frequency plots for the 90 GHz woodpile, in which the rod size is 0.40 mm with an intralayer period of 1.5 mm. As expected, in the case where there is no woodpile EM bandgap structure between the horns, the signal experiences no attenuation. When the signal is forced to go through the woodpile EM bandgap structure, the ratio of power received to power sent is also −40 dB, similar to that of the 35 GHz woodpile structure.

The 35 and 90 GHz woodpile electromagnetic bandgap structures fabricated by ISFF compare favorably to other woodpile EM bandgap substrates. For each of the woodpile structures fabricated in this work, the ratio of power received to power sent is −40 dB, or 1/10 000. This amount of attenuation was achieved with a 12-layer woodpile (three four-layer stacks). This equates to 13.3 dB per four-layer stack. Manually stacked woodpile structures by Ozbay,[6] consisted of 16 layers (four four-layer stacks) and yielded −55 dB attenuation, or 13.75d B per four-layer stack. The reliance on manual arrangement of the components of the woodpile requires the components to be fairly large (~3 mm) and lowers the operational frequency to 11–13 GHz. By contrast, the structures fabricated via ISFF benefit from the high resolution of the mold-building tool, and these woodpiles block energy at frequencies above 110 GHz. The 90 GHz alumina woodpile structures are the smallest 3-D electromagnetic bandgaps ever fabricated from low-loss materials.

(B) Planar All-Dielectric Periodic Structures: Before electrical testing, the top and bottom surfaces of the two-dimensional structures must be coated with conductive metal. The metal aligns the electric field in the array, enforcing a particular polarization within the substrate. To minimize detrimental effects to the resonator Q values, it is imperative to deposit a pure, highly conductive metal. This was accomplished by sputter coating (Hummer VI, Anatech Ltd., Alexandria, VA) a 0.5-μm layer of gold. A high-purity (99.9995%) target was used with a base pressure of 50 torr to minimize contamination.

An HP 8522D sweeping signal source network analyzer is attached to waveguides via coaxial cables. A waveguide to substrate transition is designed to transfer energy into the substrate with the planar all-dielectric resonator under test. The waveguide excites a slot in the metallized parallel plate surrounding the periodic substrate. A calibration routine is run to eliminate the loss and reflection up to the end of the waveguides; therefore, the measurements are only for the substrate itself. The peak in transmission through the substrate is then related to the Q of the resonator using Eq. (3) where the half power frequencies are taken at −3 dB down from the peak.

$$\frac{1}{Q_{UNLOADED}} = \frac{1}{\left(\frac{f_0}{f_1 - f_2}\right)} = \frac{1}{Q_{DIELECTRIC}} + \frac{1}{Q_{METAL}} + \frac{1}{Q_{LEAKAGE}} \tag{3}$$

The transmission versus frequency data for a 2-D defect resonator fabricated by ISFF is shown in Fig. 12. The structure consists of 1.1-mm rods in a square array of spacing 3.3 mm. The centermost rod in the array is missing. The results of the measurements show that the measured unloaded Q was 1365 for the structure that had a resonance at 30.7 Ghz. Calculations (HFSS, Ansoft) for these structures, simulated as alumina rods in air without the presence of the parallel plates, yield Q values of 1500. The most prominent loss mechanism (and thus the most damaging to Q) in the resonator is the loss of the dielectric of the substrate. The dielectric loss is directly related to the amount of field stored in the dielectric, as well as the loss tangent of the dielectric.

In an all-dielectric EBG resonator in which the substrate is made of dielectric rods in air, the fields are only partially stored in the dielectric, the rest is stored in the air, which is lossless. This raises the $Q_{\text{Dielectric}}$ by a factor of $1/V_f$. V_f is the volume fraction of

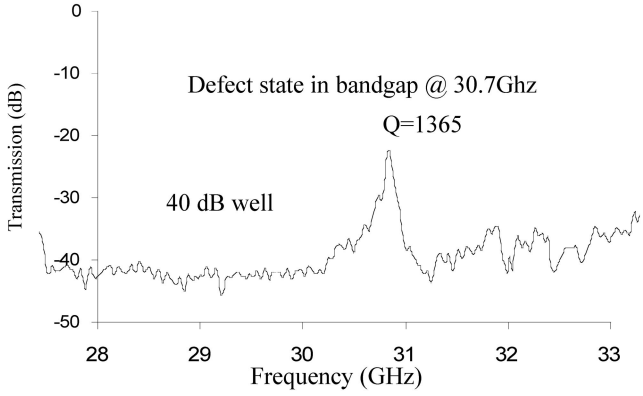

Fig. 12. Measured transmission versus frequency data for the 2-D planar, all-dielectric, defect resonator fabricated by ISFF.

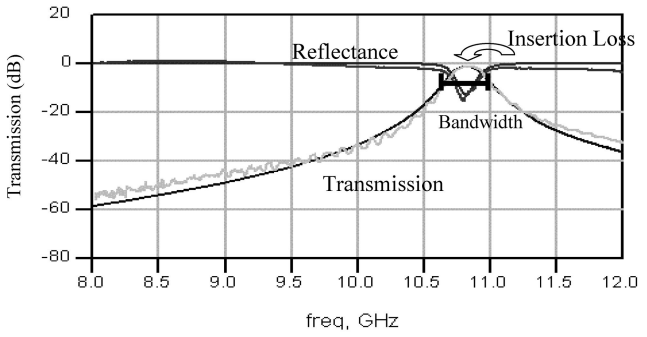

Fig. 13. Measured and simulated transmission versus frequency data for the two-pole metallo-dielectric filter fabricated by ISFF.

energy that is stored in the dielectric and is referred to as the filling fraction. The new $Q_{Dielectric}$ for the EBG structure is described by

$$Q_{Dielectric} = \frac{1}{V_f \cdot \tan \delta} \quad (4)$$

The filling fraction of the square lattice is found to be ~33%. Therefore, the $Q_{Dielectric}$ is increased by a factor of three relative to a homogeneous substrate. The presence of the plates allow more field to be stored in the dielectric rather than in the air and cause a degradation of the *Q*. The plates were polished down to minimize the effect of their thickness, but also to reduce the surface roughness. Internal features with rough surfaces cannot be polished and may contribute to the overall loss of the structure. The correlation with theoretical predictions of the *Q* values of these structures show the quality of the alumina after processing and are superior to that of the previously reported lower frequency structures machined out of Duroid.[8]

(3) Metallo-dielectric Structures

The transmission versus frequency data for a two-pole metallo-dielectric band pass filter fabricated by ISFF is shown in Fig. 13. This structure consists of a rectangular array of 0.9 mm radius holes which are then coated with metal. The period in *x* is 3.1 mm and the period in *y* is 4.0 mm. Two holes are missing (replaced with dielectric), and they are separated by two *x* spacings. The entire part, including the inner surface of the holes, is coated with a conducting layer of gold.

The bandwidth (width of the frequency window of the filter at half power (−3 dB)) of the structure is ~2.05% around a center frequency of ~10.71 GHz. The insertion loss, or the gap by which peak transmission fails to reach 0 dB (no attenuation in signal strength), was found to be ~1.05 dB. An ideal filter will have an infinitely sharp sidewall to the bandwidth and zero insertion loss. This is an unachievable goal because of the losses that are inherent in the resonators that comprise the building blocks of the filter. The losses in the resonators set the limits of filter performance, specifically the trade-off between the insertion loss and the bandwidth. The superior measured values of insertion loss and filter bandwidth for this structure relative to similar two-pole filters fabricated out of Duroid[26] are a direct result of the low dielectric loss of the ISFF alumina.

An equivalent circuit was constructed in which specific elements in series mimic electrical behavior of the substrate, for simulation purposes. A simple parallel resistor-inductor-capacitor

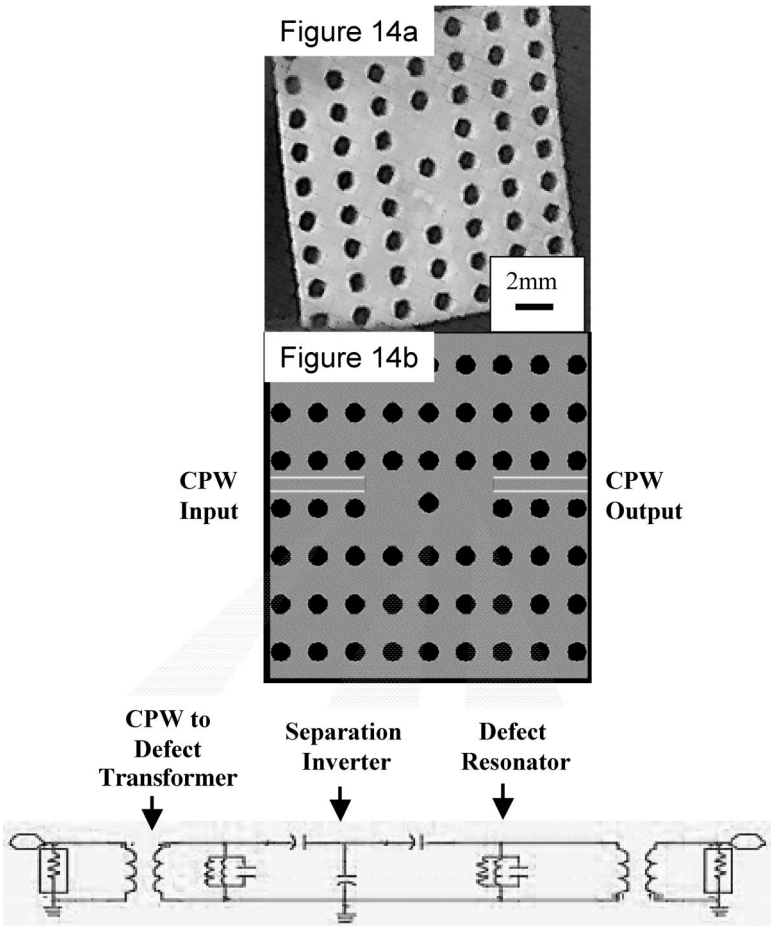

Fig. 14. (a) Image of the two-pole metallo-dielectric filter fabricated by ISFF; (b) schematic of a two-pole filter with defined coplanar waveguide lines and equivalent circuit used in the simulations.

(RLC) circuit acts as the resonator in the equivalent circuit structure.

An optical image of the fabricated two-pole metallo-dielectric filter is shown in Fig. 14(a). A schematic of the coplanar waveguide lines is illustrated in Fig. 14(b) along with the circuit elements which are used to model the overall behavior of the filter. The Q of the metallo-dielectric structure is ascertained by altering the parameters of the equivalent circuit to achieve a matched simulation of insertion loss, bandwidth, and center frequency. The Q of the resonators in the metallo-dielectric structure is known from the Q in the RLC circuits that mimic them, specifically $Q_{\text{UNLOADED}} = R/\omega l$. Through the equivalent circuits, the Q of the ISFF structure is calculated to be 644.

In contrast to the all-dielectric resonator, all the electric field in a metallo-dielectric is stored in the dielectric; therefore, the dependence on the loss tangent is even greater. Simulations show that thick substrates have potential for Q values approaching 1400 because they have more volume in which to store energy. The Q of this particular ISFF structure is part limited by its thinness. Surface roughness in the dielectric may further degrade Q by causing losses in the metal layers.

Eigenvalue analysis (Ansoft HFSS) of the resonator structure predicts a Q of 645. The major assumption of the HFSS code is that the dielectric substrate is extremely high quality, with a loss tangent on the order of 0.0001. The good agreement between the Q calculated from the equivalent RLC circuit analysis of the measured ISFF part and the Q from the HFSS simulations verifies that the alumina substrate fabricated by ISFF is high quality, low-loss material.

IV. Conclusions

Indirect solid freeform fabrication has proven to be a suitable technique for the shaping of advanced designs of periodic dielectric structures. A low-viscosity, high-solids loading suspension polymerization casting formulation has been developed and applied. Processing parameters such as mold fabrication, slurry rheology, curing, and binder burnout are detailed. Performance of the fabricated periodic dielectric resonators and filters was verified via high-frequency testing. Through ISFF, it is possible to realize complex geometry, low-loss, high-frequency designs not possible with conventional manufacturing methods.

References

[1]E. Yablonovitch, "Inhibited Spontaneous Emission in Solid State Physics and Electronics," *Phys. Rev. Lett.*, **58**, 20 2059–62 (1987).

[2]E. Yablonovitch, T. J. Gmitter, R. D. Meade, A. M. Rappe, K. D. Brommer, and J. D. Joannopoulous, "Donor and Acceptor Modes in Photonic Band Structure," *Phys, Rev. Lett.*, **67**, 3380 (1991).

[3]E. Yablonovitch and T. J. Gmitter, "Photonic Band Structure: The Face Centered Cubic Case," *Phys. Rev. Lett.*, **63**, 18 1950–53 (1989).

[4]E. Ozbay, G. Tuttle, M. Sigalas, C.M. Soukoulis, and K. M. Ho, "Defect Structures in a Layer by Layer Photonic Band Gap Crystal," *Phys. Rev. B*, **51**, 20 (1995).

[5]E. Ozbay, A. Abeyta, G. Tuttle, M. Tringides, R. Biswas, C. T. Chan, C. M. Soukoulis, and K. M. Ho, "Measurement of a Three-Dimensional Photonic Band Gap in a Crystal Structure Made of Dielectric Rods," *Phys. Rev. B*, **50** [3] 1945–48 (1994).

[6]E. Ozbay, E. Michel, G. Tuttle, R. Biswas, M. Sigalis, and K. M. Ho, "Micromachined Millimeter-Wave Photonic Band-Gap Crystals," *Appl. Phys. Lett.*, **64**, [16] 2059–61 (1994).

[7]S. Y. Lin, J. G. Fleming, D. L. Hetherington, B. K. Smith, R. Biswas, K. M. Ho, M. M. Sigalis, W. Zubrzycki, and S. R. Kurtz, "A Three Dimensional Photonic Crystal Operating at Infrared Wavelengths," *Nature (London)*, **394**, 251–53 (1998).

[8]W. J. Chappell, M. P. Little, and L. P. B. Katehi, "High Q Two-Dimensional Defect Resonators: Measured and Simulated," *IEEE MTT-S Int. Microwave Symp Dig.*, **3**, 1437–40 (2000).

[9]W. J. Chappell, C. J. Reilly, J. W. Halloran, L. P. B. Katehi,"Ceramic Sythetic Substrates Using Sold Free Form Fabrication," *IEEE Transactions on Microwave Theory Tech.*, **51** [3] (2003).

[10]M. Mott and J.G. Evans, "Solid Freeforming of Silicon Carbide by Inkjet Printing Using a Polymeric Precursor," *J. Am. Ceram. Soc.*, **84** [2] 307–13 (2001).

[11]K. A. M. Seerden, N. Reis, B. Derby, P. S. Grant, J. W. Halloran, and J. R. G. Evans, "Direct Ink-jet Deposition of Ceramic Green Bodies: I-Formulation of Build Materials"; pp. 141–46 in *Symposium V, Solid Freeform and Additive Fabrication*, Proceedings of the Materials Research Society Fall Meeting, Boston, MA, 1998; The Materials Research Society: Warrendale, PA, 1999.

[12]M. J. Wright and J. G. Evans, "Ceramic Deposition Using an Electromagnetic Jet Printer Station," *J. Mater. Sci. Lett.*, **18** [2] 99–101 (2001).

[13]M. Mott, J.-H. Song, and J. G. Evans, "Microengineering of Ceramics by Direct Ink-Jet Printing," *J. Am. Ceram. Soc.*, **82** [7] 1653–58 (1999).

[14]T. McNulty, D. Shanefield, S. Danforth, and A. Safari, "Dispersion of Lead Zirconate Titanate for Fused Deposition of Ceramics," *J. Am. Ceram. Soc.* **82** [7] 1757–60 (1999).

[15]A. Bandyopadhyay, R. K. Panda, V. F. Agarwala, S. C. Danforth, and A. Safari, "Processing of Piezocomposites by Fused Deposition Technique," *J. Am. Ceram. Soc.*, **80** [6] 1366–72 (1997).

[16]K. Venkataswamy, R. Waack, B. E. Novich, and J. W. Halloran, "Forming Whisker Reinforced Sintered Ceramics with Polymerizable Binder Precursors," U. S. Pat. No. 4 978 643, 1990.

[17]T.-M. Chu, "Solid Freeform Fabrication of Biomaterials," Ph.D. Thesis, University of Michigan, Ann Arbor, MI, 1999.

[18]C. Young, O. O. Omatete, M. A. Janney, and P. A. Menchhofer, "Gelcasting of Alumina," *J. Am. Ceram. Soc.*, **74** [3] 612 (1991).

[19]T-C. Chu and J. W. Halloran, "Curing of Highly Loaded Ceramic Suspension in Acrylates," *J. Am. Ceram. Soc.* **83** [10] 2375–80 (2000).

[20]K. S. Anseth and C. N. Bowman, "Kinetic Gelation Model Prediction of Crosslinked Polymer Network Microstructure," *Chem. Eng. Sci.*, **49** [14] 2207 (1994).

[21]I. M. Krieger and T. J. Dougherty, "A Mechanism for Non-Newtonian Flow in Suspension of Rigid Spheres," *Trans. Soc. Rheol.*, **3**, 137–52 (1959).

[22]H. Barnes, J. Hutton, and K. Walters, "Rheology of Suspensions"; pp. 115–39 in *An Introduction to Rheology*. Edited by H. Barnes. Elsevier, New York, 1989.

[23]L. Bergstrom, "Rheology of Concentrated Suspensions"; pp. 193–239 in *Surface and Colloid Chemistry in Advanced Ceramic Processing*. Edited by R. J. Pugh and L. Bergstrom. Marcel Dekker, New York, 1994.

[24]T.-M. Chu and J. W. Halloran,"High Temperature Flow Behavior of Ceramic Suspensions," *J. Am. Ceram. Soc.*, **83** [9] 2189–95 (2000).

[25]D. Richerson, *Modern Ceramic Engineering*, Marcel Dekker, New York, 1992.

[26]W. J. Chappell, M. P. Little, and L. P. B. Katehi, "High Isolation, Planar Filters Using EBG Substrates," *IEEE Microwave Wireless and Components Lett.*, **11** [6] 246–48 (2001). □